

ORIGINAL PAPER

Implementation of the electrohydrodynamics' perfect dielectric model in OpenFOAM®

Stefan A. Bošković¹ | Aleksandar Karač² | Slobodan B. Vrhovac³ | Aleksandar Belić³ | Ranko Bugarski⁴

¹Innovation Center of the Faculty of Technology and Metallurgy in Belgrade Ltd., Karnegijeva 4, 11120 Belgrade, Serbia

²Polytechnic Faculty, University of Zenica, Fakultetska 1, 72000 Zenica, Bosnia and Herzegovina

³University of Belgrade, Institute of Physics Belgrade, Pregrevica 118, 11080 Belgrade, Serbia

⁴University of Belgrade, Faculty of Technology and Metallurgy, Karnegijeva 4, 11120 Belgrade, Serbia

Correspondence

Stefan Bošković, Innovation Center of the Faculty of Technology and Metallurgy in Belgrade Ltd., Karnegijeva 4, 11120 Belgrade, Serbia
Email: sboskovic@tmf.bg.ac.rs

Abstract

The electrohydrodynamics' (EHD) perfect dielectric model was added into computational fluid dynamics (CFD) software OpenFOAM® in order to improve its usability for the EHD field and specifically for the mentioned model. Based on the investigated literature, it can be said that this is the most complete implementation of the said model. Two sets of numerical simulations with two different fluids are presented and analyzed. One set is one-dimensional. The other set is with a drop of one fluid surrounded by other fluid. Oscillations can be observed with certain expressions or calculation strategies for the electrostrictive force, and used for disregarding them. Results that are closer to analytical predictions can be obtained by using appropriate expression for the dielectric force. The electrostrictive force was implemented not only for nonpolar, but also for polar fluids, and it is shown that it might significantly influence the drop deformation. Calculated and analytically predicted drop deformations were close or comparable even up to around 0.25, what is significantly higher and different from a previous study made by other authors. Different expressions for the electric permittivity and usage of limiters for volume fractions were investigated. Conclusions from this paper can be transferred to more complicated models.

Keywords: electrohydrodynamics; EHD; CFD; OpenFOAM®; perfect dielectric model; electrostrictive force

1. INTRODUCTION

Electrohydrodynamics (EHD) is a part of physics dedicated to motion of a liquid inside an electric field (López-Herrera, Popinet, & Herrada 2011). EHD already exists for some time, based on the already published articles and books, and it can be used for certain amount of chemical engineering processes. Some of them are separations (Ptasinski & Kerkhof 1992), electrospinning and electro-spraying, which has already found certain number of applications, see e.g. (Bošković & Bugarski 2019). Electrostatic extrusion, which is a process in which electric field is used, has already been used and analyzed by our groups (Bugarski et al. 1994; Bugarski, Smith, Wu, & Goosen 1993; Manojlovic, Djonlagic, Obradovic, Nedovic, & Bugarski 2006; Poncelet, Babak, Neufeld, Goosen, & Burgarski 1999; Poncelet et al. 1994; Poncelet, Neufeld, Goosen, Burgarski, & Babak 1999). Usage of Computa-

tional Fluid Dynamics (CFD) was also started (Boskovic, Karac, Vrhovac, Belic, & Bugarski 2022), which is expected to allow better predictions of outcomes of the electrostatic extrusion process and also be applicable and usable for other processes. It was stated in Thirumalaisamy, Natarajan, and Dalal (2018) that the number of EHD implementations was limited at that moment. Since not many years have passed, it can be said that the situation is still similar. Also, since the perfect dielectric model is not the only model in EHD, the number of its implementations is even more limited. Because of these facts and the facts that the perfect dielectric model (Boskovic et al. 2022; Munoz 2015; Supeene, Koch, & Bhattacharjee 2008) can be considered simple, can be upgraded to more complex models and can be used for improving EHD calculations, it was decided to start with this model. Fluids in which polarization of molecules happens, while ohmic

conduction does not happen, are considered perfect dielectrics (Boskovic et al. 2022). The perfect dielectric model was implemented in the CFD software called OpenFOAM® (version 8), which utilizes the Finite Volume Method (FVM) (Moukalled, Mangani, & Darwish 2016) and also the Volume of Fluid (VoF) method (Andersson et al. 2011). A solver for two isothermal, incompressible and immiscible fluids (interFoam) was expanded. If this solver is used, for example, the Interface Compression (IC) or the Piecewise-Linear Interface Calculation (PLIC) corrected scheme can be used for interface reconstruction (Boskovic et al. 2022). The quality of the implementation was checked with a set-up with a drop (Supeene et al. 2008), which could be by far the most frequently used in EHD and for which it can be said that it is complex because there is fluid flow, and also with a one-dimensional set-up, which was chosen because it was noticed that it is appropriate for demonstration of one problem. Based on the investigated literature, the perfect dielectric model presented here is the first one in which the electrostrictive force (second of the two electric forces) is not overlooked (Boskovic et al. 2022), and the implementation presented here is the first two-phase implementation that includes the mentioned force in all combinations of fluid polarities, while possible effects of this force were analyzed in the following way for the first time. This model and its implementation can be used for chemical engineering processes when appropriate fluids are present without any modification, after adjusting the used geometry and fluid properties. This is analogous to the fact that the original solver can be used for different fluid flows in different geometries. Following this work, the possible future research that could further contribute to the chemical engineering field can be further experimental investigation of the electrostrictive force and the investigation of the leaky dielectric model together with an improvement of its implementations that could allow better predictions for even more fluids. This research path can be expected to lead to better equipment sizing and certain increase of the industrial applications of the electrospray, electrospinning and possibly other processes in which an electric field is used. The paper is organized in the following way: the equations and expressions used for the implemented model are given in the next section, while the results of simulations with their analysis are given afterwards in the following section for both mentioned set-ups.

2. MATHEMATICAL MODEL

The Navier-Stokes equation that was solved was equal to (Boskovic et al. 2022):

$$\frac{\partial(\rho U)}{\partial t} + \nabla \cdot (\rho U U) - \nabla \cdot (\mu \nabla U) = \rho g - \nabla p + F_s + F_C + F_{\text{oeI}} \quad (1)$$

where ρ represents the mass density, U the velocity, t the time, μ the dynamic viscosity, g the gravitational acceleration, p the pressure, F_s the surface tension force, F_C the Coulombic force, F_{oeI} other electric forces. The Coulombic force does not exist in this model, so it was set to be equal to a zero vector, but is included to allow usage of a more complicated model in the same application. F_{oeI} was either equal to the dielectric force (F_{diel}) or to the sum of F_{diel} and the electrostrictive force (F_{els}). Equations for these two last forces can be derived from the Maxwell stress tensor (Boskovic et al. 2022). Calculation of F_C and F_{oeI} was placed in the solver just before the calculation of p and U .

2.1. Calculation of the dielectric force

The dielectric force was calculated using one of the following two expressions (Boskovic et al. 2022):

$$F_{\text{diel}} = R \left\{ -\frac{1}{2} (|E|^2)_f [n_f \cdot (\nabla \epsilon)_f] |S_f| \right\} \quad (2)$$

$$F_{\text{diel}} = R \left\{ -\frac{1}{2} |n_f \cdot (\nabla \phi)_f|^2 [n_f \cdot (\nabla \epsilon)_f] |S_f| \right\} \quad (3)$$

where R represents the reconstruction function (see below), E the electric field strength, n the normal unit vector, ϵ the electric permittivity, S the surface area vector, ϕ the electric potential, while subscript f stands for the cell face.

2.2. Calculation of the electrostrictive force

In literature, the following equation can be found for the electrostrictive force (Lastow & Balachandran 2006; Reddy & Esmaeeli 2009; Torchigin & Torchigin 2013):

$$F_{\text{els}} = \nabla p_{\text{els}} = \nabla \left[\frac{1}{2} \rho \left(\frac{\partial \epsilon}{\partial \rho} \right)_T |E|^2 \right] \quad (4)$$

where p_{els} is the electrostriction pressure, T is the temperature. In Stratton (2007), a simplification for non-polar liquids can be found (Reddy & Esmaeeli 2009). So, for the electrostrictive force, either the following equation was used (Reddy & Esmaeeli 2009; Stratton 2007):

$$F_{\text{els}} = \nabla \left[\frac{(\epsilon - \epsilon_0)(\epsilon + 2\epsilon_0)}{6\epsilon_0} |E|^2 \right] \quad (5)$$

where ϵ_0 is the vacuum electric permittivity; or its variant that uses cell face values:

$$F_{\text{els}} = R \left\{ \left\{ n_f \cdot \left\{ \nabla \left[\frac{(\varepsilon - \varepsilon_0)(\varepsilon + 2\varepsilon_0)}{6\varepsilon_0} |E|^2 \right] \right\}_f \right\} |S_f| \right\} \quad (6)$$

An expression for polar dielectrics that was investigated is Kunti, Bhattacharya, and Chakraborty (2017); Shneider and Pekker (2013):

$$F_{\text{els},k} = \nabla \left(\frac{c_{\text{els},k} \varepsilon_k}{2} |E|^2 \right) \quad (7)$$

where c_{els} is an empirical factor (Shneider & Pekker 2013), subscript k denotes the polar dielectric k ; while its variant that uses cell face values is:

$$F_{\text{els},k} = R \left\{ \left\{ n_f \cdot \left[\nabla \left(\frac{c_{\text{els},k} \varepsilon_k}{2} |E|^2 \right) \right]_f \right\} |S_f| \right\} \quad (8)$$

Combinations of fluid types that can be encountered are either that both fluids are nonpolar or that both fluids are polar or that one fluid is polar and one is nonpolar. If both fluids are nonpolar liquids, Eqs. (5) and (6) can be used without modifications. If both fluids are polar dielectrics, Eq. (7) can be used with modification (Kunti et al. 2017; Shneider & Pekker 2013):

$$F_{\text{els}} = \nabla \left(\frac{c_{\text{els}} \varepsilon}{2} |E|^2 \right) \quad (9)$$

where c_{els} can be calculated from:

$$c_{\text{els}} = \alpha_{u1} c_{\text{els}1} + \alpha_{u2} c_{\text{els}2} \quad (10)$$

where α is the volume fraction, subscript u denotes the used type (see below), subscript j ($j=1,2$) denotes the fluid j ; while Eq. (8) can be modified similarly:

$$F_{\text{els}} = R \left\{ \left\{ n_f \cdot \left[\nabla \left(\frac{c_{\text{els}} \varepsilon}{2} |E|^2 \right) \right]_f \right\} |S_f| \right\} \quad (11)$$

For the case in which fluid 1 is polar, while fluid 2 is nonpolar, it was made available to use the expression that can be obtained from Eq. (11) if c_{els} is substituted by $c_{\text{els}1}$:

$$F_{\text{els}} = R \left\{ \left\{ n_f \cdot \left[\nabla \left(\frac{c_{\text{els}1} \varepsilon}{2} |E|^2 \right) \right]_f \right\} |S_f| \right\} \quad (12)$$

for the cell faces on which $(\alpha_{u1})_f$ is greater than 0.5, and Eq. (6) for other cell faces.

Similarly, for the case in which fluid 1 is nonpolar, while fluid 2 is polar, it was made available to use Eq. (6) for the cell faces on which $(\alpha_{u1})_f$ is greater than 0.5, and the expression that can be obtained from Eq. (11) if c_{els} is substituted by $c_{\text{els}2}$ for other cell faces.

2.3. Calculation of the electric permittivity

The electric permittivity was either calculated from:

$$\varepsilon = \alpha_{u1} \varepsilon_1 + \alpha_{u2} \varepsilon_2 \quad (13)$$

or calculated from (López-Herrera et al. 2011):

$$\varepsilon = \frac{\alpha_{u1} + \alpha_{u2}}{\frac{\alpha_{u1}}{\varepsilon_1} + \frac{\alpha_{u2}}{\varepsilon_2}} \quad (14)$$

The used volume fraction was either equal to the volume fraction calculated in the usual way for the VoF method, that is:

$$\alpha_{uj} = \alpha_j \quad (15)$$

or calculated by using limiters in a continuous way as in:

$$\alpha_{u1} = \begin{cases} l_{\alpha,low}, & \alpha_1 \leq l_{\alpha,low} \\ \alpha_1, & l_{\alpha,low} \leq \alpha_1 \leq l_{\alpha,up} \\ l_{\alpha,up}, & l_{\alpha,up} \leq \alpha_1 \end{cases} \quad (16)$$

where $l_{\alpha,low}$ is the lower α limiter, $l_{\alpha,up}$ is the upper α limiter; or in a discontinuous way as in:

$$\alpha_{u1} = \begin{cases} 0, & \alpha_1 \leq l_{\alpha,low} \\ \alpha_1, & l_{\alpha,low} \leq \alpha_1 \leq l_{\alpha,up} \\ 1, & l_{\alpha,up} \leq \alpha_1 \end{cases} \quad (17)$$

2.4. Other calculations

The electric field strength was calculated using the equation (Lastow & Balachandran 2006):

$$E = -\nabla \phi \quad (18)$$

The following equation should be satisfied (López-Herrera et al. 2011):

$$\nabla \times E = 0 \quad (19)$$

so $\nabla \times E$ was calculated for checking results (Boskovic et al. 2022).

The electric potential was calculated in the following way (Munoz 2015; Supeene et al. 2008):

$$\nabla \cdot (\varepsilon \nabla \phi) = 0 \quad (20)$$

The reconstruction function is equal to (Boskovic et al. 2022):

$$R(z_f) = \left(\sum_f S_f \frac{S_f}{|S_f|} \right)^{-1} \cdot \left(\sum_f z_f \frac{S_f}{|S_f|} \right) \quad (21)$$

where z represents a variable. The reconstruction function already present in the OpenFOAM® was used

to reconstruct cell center values starting from face values (Boskovic et al. 2022).

The time step length was calculated using the Courant number and the interface Courant number, which were already present in the starting solver, and the electric Courant number (Co_{el}) (Boskovic et al. 2022):

$$Co_{el} = \frac{|E|\sqrt{\varepsilon/\rho}}{\delta x/\delta t} \quad (22)$$

where x represents an axis, and also the interface electric Courant number, which were added to the solver.

3. RESULTS AND DISCUSSION

All systems consisted of two fluids (fluid 1 and fluid 2) with interfacial tension of 0.1 N m^{-1} . The gravity acceleration was equal to $\mathbf{0}$. Both fluids had the same mass density of 1000 kg m^{-3} and the same kinematic viscosity of $10^{-6} \text{ m}^2 \text{ s}^{-1}$. The electric permittivity of fluid 1 was equal to $2 \times 10^{-8} \text{ F m}^{-1}$ and of fluid 2 to $2 \times 10^{-9} \text{ F m}^{-1}$. These two fluids are located between wall 1 with the electric potential ϕ_{w1} and wall 2 with $\phi_{w2}=0 \text{ V}$. The electrostrictive force was neglected in most of the calculations. When is used and when it was needed, it was characterized by $c_{els1}=0.1$ and $c_{els2}=0.1$. These values were chosen because they were deemed as great enough for influencing results. If other values of parameters were used, it is stated explicitly in the text. Either the Multicut Piecewise-Linear Interface Calculation (MPLIC) or the IC corrected scheme was used for calculating volume fractions. Meshes were static. Paraview (with paraFoam) was used for displaying results. For all four Courant numbers, 0.1 was used as a target maximum value in order to improve the accuracy of the result. The curl of the electric field strength was calculated, but it was mentioned only when it was deemed as important. The set of equations or expressions that was finally obtained uses Eq. (1) (the Navier-Stokes equation), Eq. (3) (the dielectric force), Eq. (13) (the electric permittivity), Eq. (15) (the used volume fraction), Eq. (18) (the electric field strength), Eq. (19) (used indirectly for checking results), Eq. (20) (the electric potential), Eq. (21) (the reconstruction function), Eq. (22) (the electric Courant number), while addition of an appropriate expression for the electrostrictive force could be the best approach. Also, if this set of expressions is used, the used volume fractions can be bypassed because they are no longer needed.

3.1. One-dimensional analysis

Quick qualitative comparison of expressions used for the electrostrictive force was done by using a one-dimensional set-up. An analytical equation that would account for all

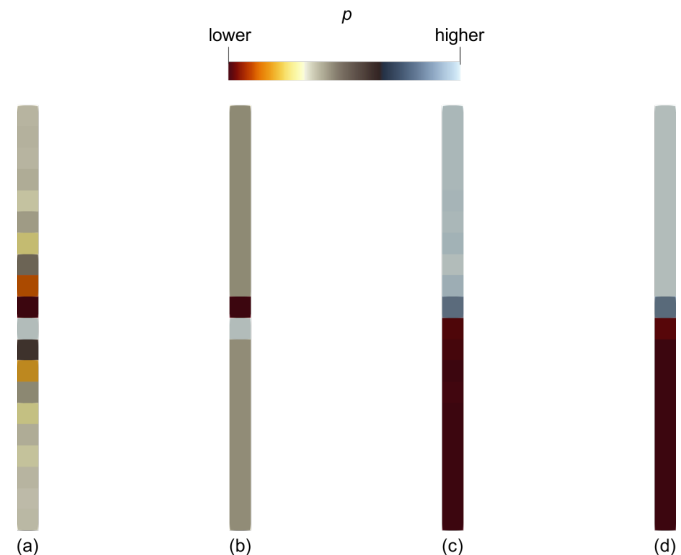


Figure 1. The pressure in the area close to the interface (from $x=0.4 \text{ mm}$ to $x=0.6 \text{ mm}$) at 0.02 s when (a) Eq. (5), (b) Eq. (6), (c) Eq. (9), (d) Eq. (11) was used for the electrostrictive force (the color map was adjusted for every case independently).

the forces for this set-up was not found in literature. Wall 1 with $\phi_{w1}=150 \text{ V}$ was placed at $x=1 \text{ mm}$. Wall 2 was at $x=0$. Fluid 2 was placed in the top half of the geometry, while fluid 1 was below it (in the bottom half). The mesh consisted of 100 equal cells, while 0.02 s were simulated. The dielectric force, the electric permittivity, and the used volume fraction were given by Eqs. (3), (13), and (15), respectively. The IC scheme was used. The pressure in the area close to the interface when Eqs. (5), (6), (9), and (11) were used can be seen in Figure 1. Oscillations of the pressure, which indicate numerical instability, can be seen when only volume fields were present in the expressions for the electrostrictive force (i.e. when Eqs. (5) and (9) were used). Such oscillations were not present when cell face values (with their reconstruction) were used in those expressions. Because of this, usage of Eqs. (5) and (9) for the electrostrictive force is disregarded and usage of expressions for the electrostrictive force in which cell face values (with their reconstruction) are present could be recommended. This is in accordance with (Boskovic et al. 2022).

3.2. Drop deformation analysis

For a case when a dielectric drop is in a dielectric media, an equation was derived for calculating the deformation of the drop when it is in an electric field (Supeene et al. 2008). The mentioned equation is (Allan & Mason 1962; Supeene et al. 2008):

$$D_{ss,df} = \frac{9}{16} \frac{r_0 \varepsilon_{sf}}{\gamma} \left(|E_0| \frac{\varepsilon_{df}/\varepsilon_{sf} - 1}{\varepsilon_{df}/\varepsilon_{sf} + 2} \right)^2 \quad (23)$$

where D is the deformation, r_0 is the starting radius of a sphere, γ is the interfacial tension, E_0 is the strength of the macroscopically uniform electric field, subscript ss denotes a steady-state, subscript df denotes the drop fluid, subscript sf denotes the surrounding fluid. It is stated in [Supeene et al. \(2008\)](#) that the problem with this approach is that it pertains to small deformations under small electric fields and that it does not apply to dynamic problems. The deformation of the drop can be calculated using ([Singh, Bahga, & Gupta 2019](#); [Supeene et al. 2008](#)):

$$D_{df} = \frac{b-a}{b+a} \quad (24)$$

where b is the length of the drop measured parallelly to the electric field, a is the length of the drop measured perpendicularly to the electric field. The strength of the macroscopically uniform electric field was calculated from the equation that can be written as:

$$|E_0| = \left| \frac{\phi_{w1} - \phi_{w2}}{l_w} \right| \quad (25)$$

where l_w is the distance between the two walls.

A change in the pressure caused by a static electric field was measured for nonpolar isotropic liquid dielectrics ([Hakim & Higham 1962](#); [Shevchenko & Hoenders 2010](#)) and is stated to be equal to ([Shevchenko & Hoenders 2010](#)):

$$\Delta p = \frac{(\varepsilon - \varepsilon_0)(\varepsilon + 2\varepsilon_0)}{6\varepsilon_0} |E|^2 \quad (26)$$

Based on the comparison of Eqs. (26) and (5), and the statement in [Taylor \(2011\)](#) that the electrostrictive force is exactly balanced by a pressure increase in the incompressible drop, it could be expected that inclusion of an expression for the electrostrictive force would result just in a pressure increase. Axially symmetric geometries, as in [Figure 2](#), were made. A drop consisting of fluid 1 was at the symmetry axis' center. Its starting radius was 25 μm , unless stated otherwise. The surrounding fluid was fluid 2. The border that is opposite to the mentioned symmetry axis was the outer wall on which the electric potential's gradient was set to $\mathbf{0}$. The symmetry axis and the outer wall were separated by a distance that was equal to $4r_0$, while other two borders (wall 1 and wall 2) were separated by l_w that was $10r_0$. Static meshes consisting of hexahedra and prisms (because of the symmetry axis) were used. Dynamic meshes were not used because of the conclusion that can be seen in ([Boskovic et al. 2022](#)). Fifty cells per $2r_0$ were set, unless stated otherwise. The width and the height used for calculations of the cells were set to be equal, while their third dimension depended on

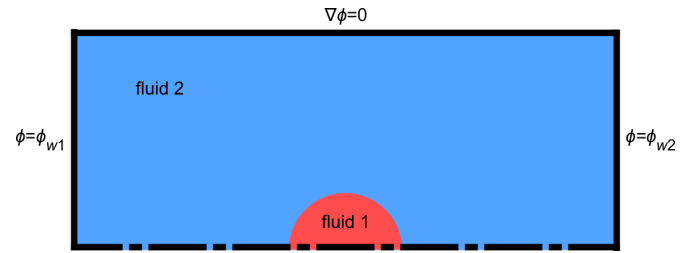


Figure 2. Axially symmetric geometry for cases in which drop deforms.

their position. When the VoF method is used, satisfactory results for an object of spherical shape are expected to be obtained if a mesh having around 20 cells per its diameter is used ([Andersson et al. 2011](#)). The place of the interface is not defined in the output of the VoF method and was determined by using a value of volume fraction equal to 0.5.

3.2.1. Comparison with other numerical calculations

In order to evaluate this implementation, results were compared to some previous calculations of other authors. In particular, a comparison with a previous study of the perfect dielectric model when two fluids are present was done ([Supeene et al. 2008](#)). Hopefully, the simulations presented here could lead to more realistic calculations that will be directly comparable to laboratory experiments. In [Supeene et al. \(2008\)](#), the calculated and the analytically predicted (Eq. (23)) drop deformations were very close for very small (up to 0.0004) deformations, while they diverged when the predicted deformation was 0.0036 or larger. This difference was attributed to non-linearity ([Supeene et al. 2008](#)). However, this difference can also be due to other causes. For example, in [Supeene et al. \(2008\)](#), no calculation of the curl of the electric field was reported, while a dynamic mesh was used, so there is a possibility that the mentioned curl was generated, as discussed in ([Boskovic et al. 2022](#)). The set-up found in [Supeene et al. \(2008\)](#) was reproduced. The electric permittivity of fluid 1 was equal to $7.0832 \times 10^{-10} \text{ F m}^{-1}$, of fluid 2 to $2.6562 \times 10^{-11} \text{ F m}^{-1}$; r_0 was equal to 1 μm , and γ to 0.03 N m^{-1} . Value of ϕ_{w1} was changed as needed. The obtained results when Eqs. (3), (13), and (15) were used for the dielectric force, the electric permittivity and used volume fractions, respectively, are shown in [Figure 3](#), where the subscript an denotes the solution from Eq. (23), and the subscript $calc$ denotes the calculated solution. Both the IC scheme and the MPLIC scheme were used for calculations. Better results were obtained with the IC scheme for lower values of the drop deformation. When the MPLIC scheme was used for the lower values

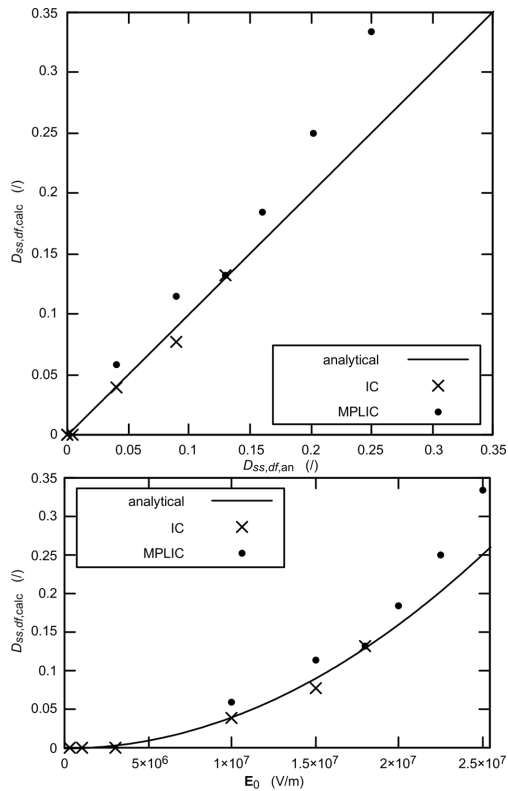


Figure 3. Obtained results for the set-up from [Supeene et al. \(2008\)](#).

of the deformation, the drop did not stay in the center and started moving towards one of the walls, while the value obtained for the case when E_0 was equal to 10 MV m^{-1} is expected to be caused mainly by spurious currents because deformations up to this value were observed with the starting (unmodified) solver without the electric field. Also, it can be said for the fact that the obtained drop deformation for 10 MV m^{-1} was below the analytical prediction when the IC scheme was used that it is just caused by the used mesh resolution and that the trend of the results is important. As the drop deformation was increased when the IC scheme was used, first small amount of the drop fluid started exiting the original drop, while the amount of the drop fluid that was exiting latter grew enough to not enable good determination of the drop dimensions. This problem was not encountered when the MPLIC scheme was used. Whether some amount of fluid would exit in reality or not is undetermined, but for the sake of comparison with Eq. (23), usage of the MPLIC scheme only for higher deformations was not seen as unjustified, while it could be said that the problem with spurious currents was apparently overcome starting at least with the 18 MV m^{-1} case. Drop deformations that are higher than the ones presented here were not obtained because the drop spread out touching both walls for the case in which E_0 was equal to 27.5 MV m^{-1} .

As can be seen from Figure 3, results that are close or comparable to Eq. (23) are obtained for the drop deformations even up to around 0.25. This is significantly different from [Supeene et al. \(2008\)](#) where it is reported that results comparable to the analytical solution were obtained for the cases in which E_0 was equal to 10 MV m^{-1} or 15 MV m^{-1} , while the calculation broke down when it was equal to 20 MV m^{-1} . Also, for the case in which the value predicted by Eq. (23) was equal to 0.0399, a value equal to 0.0400 was obtained by using the implementation presented here, while 0.0399 is 100 times greater than the highest value mentioned in [Supeene et al. \(2008\)](#) for which the obtained value was very close to the analytically predicted value according to the authors (i.e. 0.0004). Even for the case in which the predicted value was equal to 0.129, the value obtained 0.132 which is quite close. For showing the applicability of the used mesh, one simulation for the case in which the analytical prediction was equal to 0.0399 was done using the IC scheme with 22 cells per $2r_0$. The obtained drop deformation in that case was equal to 0.0431. Based on this result, it can be concluded that even less than 50 cells per $2r_0$ can be used (as could have been expected), but the quality of the results can be expected to be somewhat reduced because of the reduced mesh resolution. These results, Eq. (23) still holds for drop deformations greater than 0.0004. Also, an advantage of the implementation presented here is that the numerical breakdown similar to the one described in [Supeene et al. \(2008\)](#) was neither encountered nor is expected to be encountered.

3.2.2. Dielectric force expressions

Here, the IC scheme was used, while Eqs. (13) and (15) were used for the electric permittivity and used volume fractions, respectively. The obtained drop deformation for the case when E_0 was equal to 10 MV m^{-1} was equal to 0.0400 when Eq. (3) was used and to 0.1154 when Eq. (3) was used, while the value equal to 0.0399 can be obtained by using Eq. (23) for this case. Since it was noticed that when the dimensions of the whole geometry were reduced, the curl of the electric field strength increased inside the geometry, this could be the possible explanation for the obtained high drop deformation when Eq. (2) was used. The mentioned curl at 10^{-6} s is shown in Figure 4 when Eq. (2) was used. The implementation of Eq. (2) in OpenFOAM® uses the gradient function that is already built-in, while the implementation of Eq. (3) uses different, also built-in, function for the surface normal gradient, so the problem in the calculation of the gradient could have been bypassed this way. Because of this, Eq. (2) was disregarded and was not used for following calculations. The fact that the increase of the mentioned curl

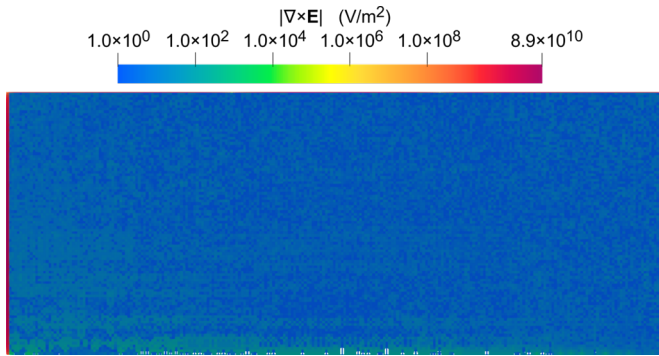


Figure 4. The curl of the electric field strength at 10^{-6} s when Eq. (2) was used (the color map was set to start from 1).

was noticed was not deemed as problematic for this study because it can be said that it is connected to the used software and its underlying calculations and because those distances are close to the ones for which fluid dynamics is stated to be inapplicable.

3.2.3. Electric permittivity expressions

When the MPLIC scheme and Eq. (15) for used volume fractions were used for the case in which \mathbf{E}_0 was equal to 20.0 MV m^{-1} , the obtained drop deformation when Eq. (13) was used for the electric permittivity was equal to 0.185, while it was equal to 0.200 when Eq. (14) was used instead. The value of the drop deformation that can be calculated from Eq. (23) is equal to 0.160, so the result obtained by using Eq. (13) was closer to this value. Because of this, because it is questionable whether Eq. (14) can be justified physicochemically, and because its form is different from the form that is usual for the VoF method, usage of Eq. (14) was disregarded.

3.2.4. Used volume fractions

Different expressions for the used volume fractions (Eqs. (16) and (17)) were tried out in the case in which \mathbf{E}_0 was equal to 22.5 MV m^{-1} , while the IC scheme was used. This case was used to check whether the mentioned exiting of the fluid could be stopped. A value equal to 0.01 was used for $l_{\alpha,low}$ and to 0.99 for $l_{\alpha,up}$.

When Eq. (17) was used, the drop was somewhat more compressed in the beginning, but at 2.75×10^{-6} s pointed tips with α_1 higher than around 0.5 were observed on both sides of the drop, while they were observed on only one side of the drop when Eq. (15) was used. Even though that it could be said that the results might have been better because they were more symmetrical, Eq. (17) did not enable usage of the IC scheme for the investigated case so it was disregarded. When Eq. (16) was

used, the drop almost spread enough to touch both walls at 2.75×10^{-6} s so it was also disregarded.

3.3. Electrostrictive force

Inclusion of Eq. (6) or of Eq. (11) did not affect the final drop deformation (equal to 0.132) when the MPLIC scheme and $\phi_{w1} = 174.3 \text{ V}$ were used, in accordance with Taylor (2011), where it is stated that the electrostrictive force does not affect the incompressible droplet shape. The obtained final drop deformation did not change even in cases in which either of the parameters c_{els1} or c_{els2} was set to be equal to 1.5 (this value was used previously in Shneider and Pekker (2013)). In Figure 5. the velocity magnitude and the calculated pressure are shown at 2.5×10^{-4} s, where it can be seen that the addition of the electrostrictive force (Eq. (6)) almost did not change the former, while it led to a noticeable change of the latter. When the IC scheme and $\phi_{w1} = 20 \text{ V}$ were used, the obtained drops for the cases in which either no equation for the electrostrictive force was used or one fluid was polar and one was nonpolar are presented in Figure 6. The obtained final drop deformations were equal to 0.00 for the former case, to -0.102 for the case in which fluid 1 was polar and fluid 2 was nonpolar and to 0.185 for the case in which fluid 1 was nonpolar and fluid 2 was polar. The fact that the electrostrictive force caused the compression of a polar drop surrounded by a nonpolar fluid is not surprising, since the dielectric force causes elongation of the drop in the direction parallel to the electric field, since the electrostrictive force has different sign from the dielectric force, and since it could be expected that the electrostrictive force has greater influence on a polar than on a nonpolar fluid. The same reasons lead to the opposite effect in the opposite case of a nonpolar drop surrounded by a polar fluid. However, the resulting compression of the polar drop in the electric field is not in accordance with the experimentally observed elongation of the water drops surrounded by oil (Berg, Lundgaard, & Abi-Chebel 2010), what could be caused by the nonexistence of the Coulombic force in the perfect dielectric model.

A possible explanation for the mentioned statement that the electrostrictive force does not change the drop deformation can be obtained by arguing that the net force that causes the electrostriction pressure in any volume is zero (Torchigin & Torchigin 2013). The changes in the deformation here presented could be seen as a numerical proof for the opposite statement mentioned in Torchigin and Torchigin (2013), and are probably due to an inhomogeneity that exists in the electrostriction pressure, causing the density force to appear. This is not surprising since in the used implementation a discontinuity in \mathbf{F}_{els} can happen around or at $(\alpha_{u1})_f = 0.5$, which is expected

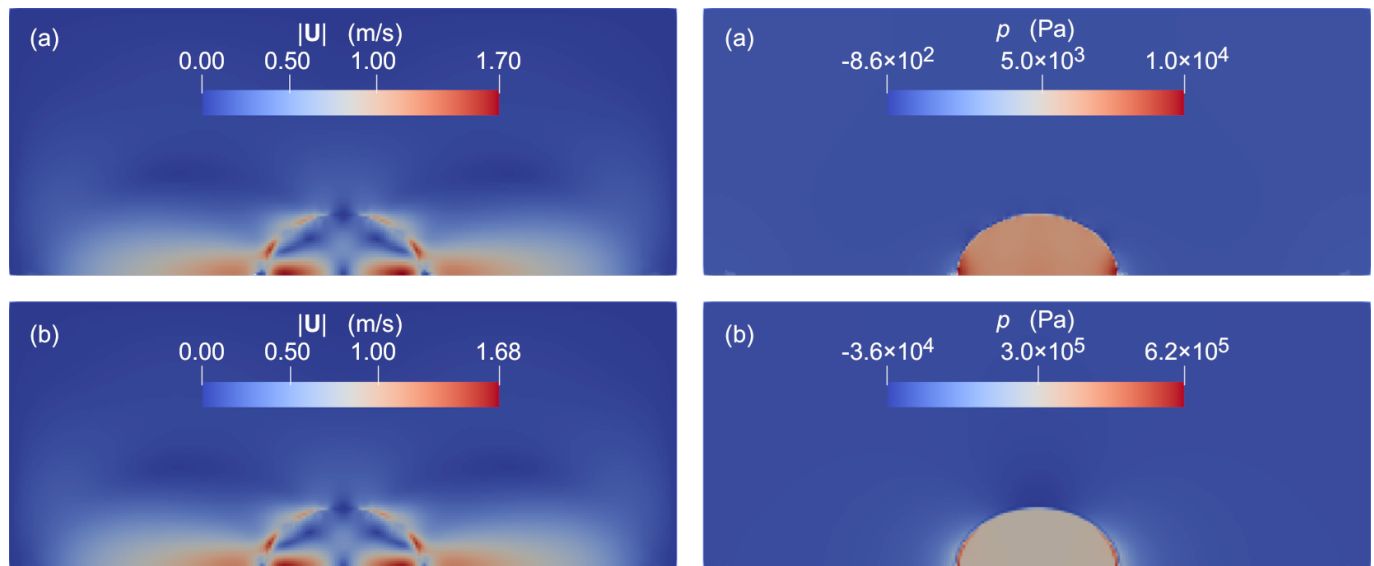


Figure 5. The velocity magnitude and the calculated pressure at 2.5×10^{-4} s (a) without any equation for the electrostrictive force, (b) when Eq. (6) was used.

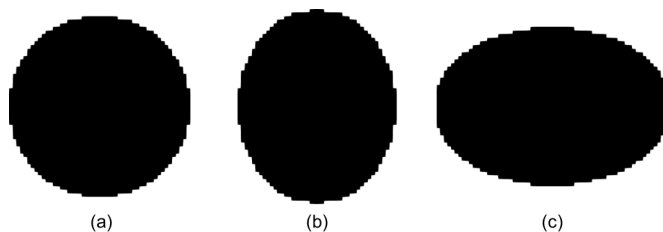


Figure 6. The obtained drop (a) without any equation for the electrostrictive force, (b) with equations corresponding to the case when fluid 1 is polar and fluid 2 is nonpolar, (c) with equations corresponding to the case when fluid 1 is nonpolar and fluid 2 is polar.

to invalidate the proof found in Torchigin and Torchigin (2013) that is based upon the integration of a function. This observation could possibly contribute to the ongoing discussions in the field of optics. It is clear that further investigation of models for the electrostrictive force is needed to clarify if the discontinuity is preferred. Inclusion of the electrostrictive force (either Eq. (6) or Eq. (11) or a more appropriate expression that uses cell face values and their reconstruction, depending on investigated fluids) in a perfect dielectric model and in other models for situations in which an electric field influences fluids could be recommended for incompressible cases even for non-polar fluids because its omission could influence the calculated pressure. Usage of the electrostrictive force in the case of compressible fluids can already be found (Shneider & Pekker 2013).

4. CONCLUSIONS

After this analysis, several conclusions can be made. Different expressions for electric forces were compared and those that could be the best were identified based on results, as discussed previously. Oscillations, which indicate numerical instability, were observed with expressions for the electrostrictive force that use cell center values only, while they were not observed with the ones that use cell face values. Inclusion of the electrostrictive force had significant effect, both influencing the calculated pressure, in accordance with Taylor (2011), and other parameters, as discussed above (Torchigin & Torchigin 2013). Different expressions for the electric permittivity and the used volume fractions were used and compared. The detailed comparison with previous calculations of drop deformations for the perfect dielectric model (Supeene et al. 2008) was presented. Significantly better agreement with analytical formula for the drop deformation (Allan & Mason 1962; Supeene et al. 2008) was found, extending up to around 0.25. The overall conclusion is that the perfect dielectric model can be incorporated in OpenFOAM® to improve its usability for electrohydrodynamics. This implementation is suitable as a starting point for more realistic models for cases in which an electric field influences fluids.

ACKNOWLEDGEMENTS

This work was supported by the Ministry of Education, Science and Technological Development of the Republic of Serbia (Contracts No. 451-03-9/2022-14/200287 and No. 451-03-9/2022-14/200135) and by Science Fund of

the Republic of Serbia (The Program IDEAS MultiPromis 7751519). The authors acknowledge funding provided by the Institute of Physics Belgrade, through the grant by the Ministry of Education, Science, and Technological Development of the Republic of Serbia.

CONFLICTS OF INTEREST

The authors did not have conflicts of interest.

NOMENCLATURE

Roman symbols

- a - length of the drop measured perpendicularly to the electric field (m)
- b - length of the drop measured parallelly to the electric field (m)
- c_{els} - empirical factor for the electrostrictive force (/)
- Co_{el} - electric Courant number (/)
- D - deformation (/)
- E - electric field strength ($V m^{-1}$)
- E_0 - strength of the macroscopically uniform electric field ($V m^{-1}$)
- F - force (N)
- F_{els} - electrostrictive force (N)
- g - gravitational acceleration ($m s^{-2}$)
- $l_{\alpha,low}$ - lower α limiter (/)
- $l_{\alpha,up}$ - upper α limiter (/)
- l_w - distance between two walls (m)
- n - normal unit vector (/)
- p - pressure (Pa)
- p_{els} - electrostriction pressure (Pa)
- R - reconstruction function
- r_0 - starting radius of a sphere (m)
- S - surface area vector (m^2)
- T - temperature (K)
- t - time (s)
- U - velocity ($m s^{-1}$)
- x - an axis (/)
- z - variable

Greek Symbols

- α - volume fraction (/)
- ϵ - electric permittivity ($F m^{-1}$)
- ϵ_0 - vacuum electric permittivity ($F m^{-1}$)
- γ - interfacial tension ($N m^{-1}$)
- μ - dynamic viscosity (Pa s)
- ϕ - electric potential (V)
- ϕ_{wj} - ϕ on wall j , $j = 1, 2$ (V)
- ρ - mass density ($kg m^{-3}$)

Subscripts

- an - analytical solution
- C - Coulombic
- $calc$ - obtained solution
- df - drop fluid
- $diel$ - dielectric
- f - cell face
- k - polar dielectric k
- oel - other electric
- s - surface tension
- sf - surrounding fluid
- ss - steady-state
- u - used type

Abbreviations

- CFD - Computational Fluid Dynamics
- EHD - electrohydrodynamics
- FVM - Finite Volume Method
- IC - Interface Compression
- MPLIC - Multicut Piecewise-Linear Interface Calculation
- PLIC - Piecewise-Linear Interface Calculation
- VoF - Volume of Fluid

REFERENCES

- Allan, R., & Mason, S. (1962). Particle behaviour in shear and electric fields i. deformation and burst of fluid drops. *Proceedings of the Royal Society of London. Series A. Mathematical and Physical Sciences*, 267(1328), 45–61. <https://doi.org/10.1098/rspa.1962.0082>
- Andersson, B., Andersson, R., Håkansson, L., Mortensen, M., Sudiyo, R., & Van Wachem, B. (2011). *Computational fluid dynamics for engineers*. Cambridge university press.
- Berg, G., Lundgaard, L. E., & Abi-Chebel, N. (2010). Electrically stressed water drops in oil. *Chemical Engineering and Processing: Process Intensification*, 49(12), 1229–1240. <https://doi.org/10.1016/j.cep.2010.09.008>
- Bošković, S., & Bugarski, B. (2019). Review of electrospray observations and theory. *J. eng. process. manag.*, 10(2). <https://doi.org/10.7251/jepm181002041b>
- Boskovic, S., Karac, A., Vrhovac, S., Belic, A., & Bugarski, B. (2022). Investigation of electrohydrodynamic calculations. *Chemical Industry*, 76(2), 65–74. <https://doi.org/10.2298/hemind211110010b>
- Bugarski, B., Li, Q., Goosen, M. F. A., Poncelet, D., Neufeld, R. J., & Vunjak, G. (1994). Electrostatic droplet generation: Mechanism of polymer droplet formation. *AIChE Journal*, 40(6), 1026–1031. <https://doi.org/10.1002/aic.690400613>
- Bugarski, B., Smith, J., Wu, J., & Goosen, M. F. A. (1993). Methods for animal cell immobilization using electrostatic droplet generation. *Biotechnology Techniques*, 7(9), 677–682. <https://doi.org/10.1007/bf00151869>

- Hakim, S. S., & Higham, J. B. (1962). An experimental determination of the excess pressure produced in a liquid dielectric by an electric field. *Proceedings of the Physical Society*, 80(1), 190–198. <https://doi.org/10.1088/0370-1328/80/1/322>
- Kunti, G., Bhattacharya, A., & Chakraborty, S. (2017). A scaling analysis for electrohydrodynamic convection with variable thermophysical and electrical properties. *International Journal of Heat and Mass Transfer*, 109, 215–222. <https://doi.org/10.1016/j.ijheatmasstransfer.2017.01.104>
- Lastow, O., & Balachandran, W. (2006). Numerical simulation of electrohydrodynamic (EHD) atomization. *Journal of Electrostatics*, 64(12), 850–859. <https://doi.org/10.1016/j.elstat.2006.02.006>
- López-Herrera, J., Popinet, S., & Herrada, M. (2011). A charge-conservative approach for simulating electrohydrodynamic two-phase flows using volume-of-fluid. *Journal of Computational Physics*, 230(5), 1939–1955. <https://doi.org/10.1016/j.jcp.2010.11.042>
- Manojlovic, V., Djonlagic, J., Obradovic, B., Nedovic, V., & Bugarski, B. (2006). Immobilization of cells by electrostatic droplet generation: a model system for potential application in medicine. *International Journal of Nanomedicine*, 1(2), 163–171. <https://doi.org/10.2147/nano.2006.1.2.163>
- Moukalled, F., Mangani, L., & Darwish, M. (2016). *The finite volume method in computational fluid dynamics*. Springer International Publishing. <https://doi.org/10.1007/978-3-319-16874-6>
- Munoz, C. N. (2015). *Computational modelling of electrohydrodynamic atomization* (Unpublished doctoral dissertation). The University of Manchester (United Kingdom).
- Poncelet, D., Babak, V., Neufeld, R., Goosen, M., & Burgarski, B. (1999). Theory of electrostatic dispersion of polymer solutions in the production of microgel beads containing biocatalyst. *Advances in Colloid and Interface Science*, 79(2-3), 213–228. [https://doi.org/10.1016/S0001-8686\(97\)00037-7](https://doi.org/10.1016/S0001-8686(97)00037-7)
- Poncelet, D., Neufeld, R., Bugarski, B., Amsden, B. G., Zhu, J., & Goosen, M. F. A. (1994). A parallel plate electrostatic droplet generator: Parameters affecting microbead size. *Applied Microbiology and Biotechnology*, 42(2-3), 251–255. <https://doi.org/10.1007/bf00902725>
- Poncelet, D., Neufeld, R. J., Goosen, M. F. A., Burgarski, B., & Babak, V. (1999). Formation of microgel beads by electric dispersion of polymer solutions. *AIChE Journal*, 45(9), 2018–2023. <https://doi.org/10.1002/aic.690450918>
- Ptasinski, K. J., & Kerkhof, P. J. A. M. (1992). Electric field driven separations: Phenomena and applications. *Separation Science and Technology*, 27(8-9), 995–1021. <https://doi.org/10.1080/01496399208019021>
- Reddy, M. N., & Esmaeeli, A. (2009). The EHD-driven fluid flow and deformation of a liquid jet by a transverse electric field. *International Journal of Multiphase Flow*, 35(11), 1051–1065. <https://doi.org/10.1016/j.ijmultiphaseflow.2009.06.008>
- Shevchenko, A., & Hoenders, B. J. (2010). Microscopic derivation of electromagnetic force density in magnetic dielectric media. *New Journal of Physics*, 12(5), 053020. <https://doi.org/10.1088/1367-2630/12/5/053020>
- Shneider, M. N., & Pekker, M. (2013). Dielectric fluid in inhomogeneous pulsed electric field. *Physical Review E*, 87(4). <https://doi.org/10.1103/physreve.87.043004>
- Singh, R., Bahga, S. S., & Gupta, A. (2019). Electrohydrodynamics in leaky dielectric fluids using lattice boltzmann method. *European Journal of Mechanics - B/Fluids*, 74, 167–179. <https://doi.org/10.1016/j.euromechflu.2018.11.011>
- Stratton, J. A. (2007). *Electromagnetic theory* (Vol. 33). John Wiley & Sons.
- Supeene, G., Koch, C. R., & Bhattacharjee, S. (2008). Deformation of a droplet in an electric field: Nonlinear transient response in perfect and leaky dielectric media. *Journal of Colloid and Interface Science*, 318(2), 463–476. <https://doi.org/10.1016/j.jcis.2007.10.022>
- Taylor, J. M. (2011). *Optical binding phenomena: Observations and mechanisms*. Springer Berlin Heidelberg. <https://doi.org/10.1007/978-3-642-21195-9> doi: 10.1007/978-3-642-21195-9
- Thirumalaisamy, R., Natarajan, G., & Dalal, A. (2018). Towards an improved conservative approach for simulating electrohydrodynamic two-phase flows using volume-of-fluid. *Journal of Computational Physics*, 367, 391–398. <https://doi.org/10.1016/j.jcp.2018.04.024>
- Torchigin, V., & Torchigin, A. (2013). Interrelation between various types of optically induced forces. *Optics Communications*, 301-302, 147–151. <https://doi.org/10.1016/j.optcom.2013.03.041>